

Supporting Information for

**Metal organic frameworks from extended, conjugated
pentiptycene-based ligands**

Angela K. Crane, Nicholas G. White and Mark J. MacLachlan*

*Department of Chemistry, University of British Columbia, 2036 Main Mall,
Vancouver, British Columbia, Canada, V6T 1Z1*

Contents	1
NMR spectra of new organic compounds	2
Powder X-ray diffraction of PMOFs	6
Thermogravimetric analysis of PMOFs	8
Reaction of 1^{2H} with $Zn(NO_3)_2 \cdot 6H_2O$	9

NMR spectra of new organic compounds

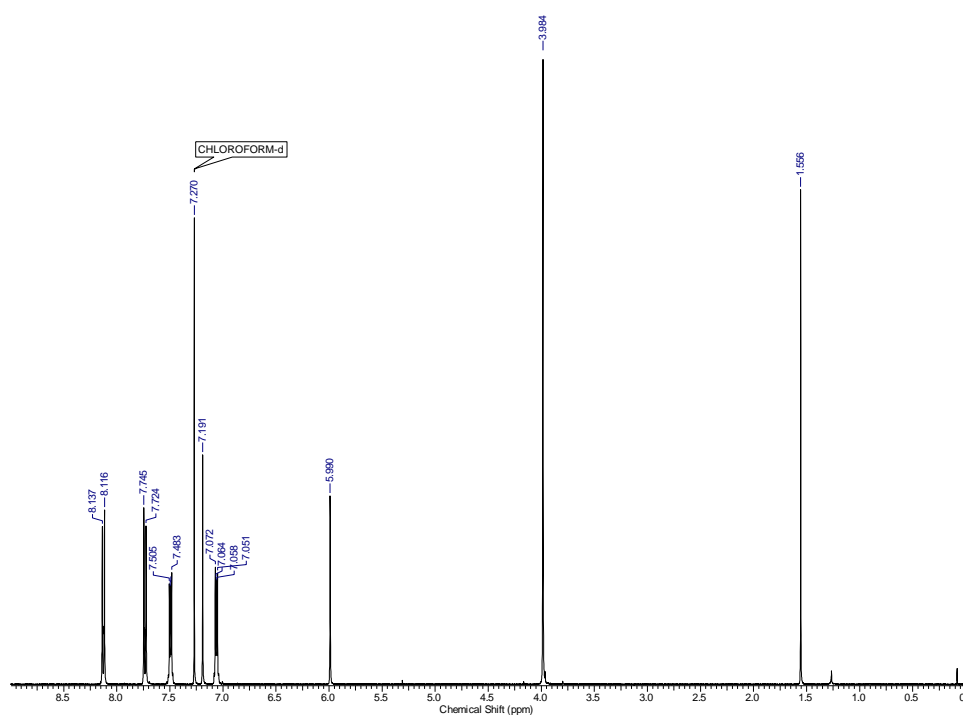


Figure S1. ^1H NMR spectrum of triptycene diester **5** (CDCl_3 , 298 K, 400 MHz; peak at 1.538 ppm corresponds to residual water in the solvent).

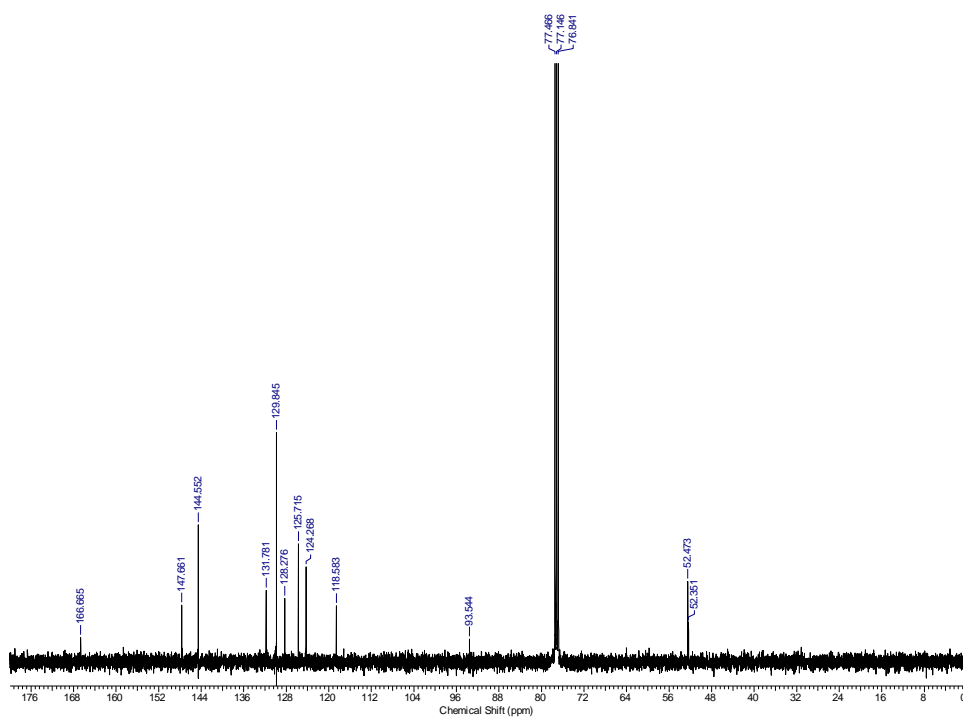


Figure S2. ^{13}C NMR spectrum of triptycene diester **5** (CDCl_3 , 298 K, 100 MHz).

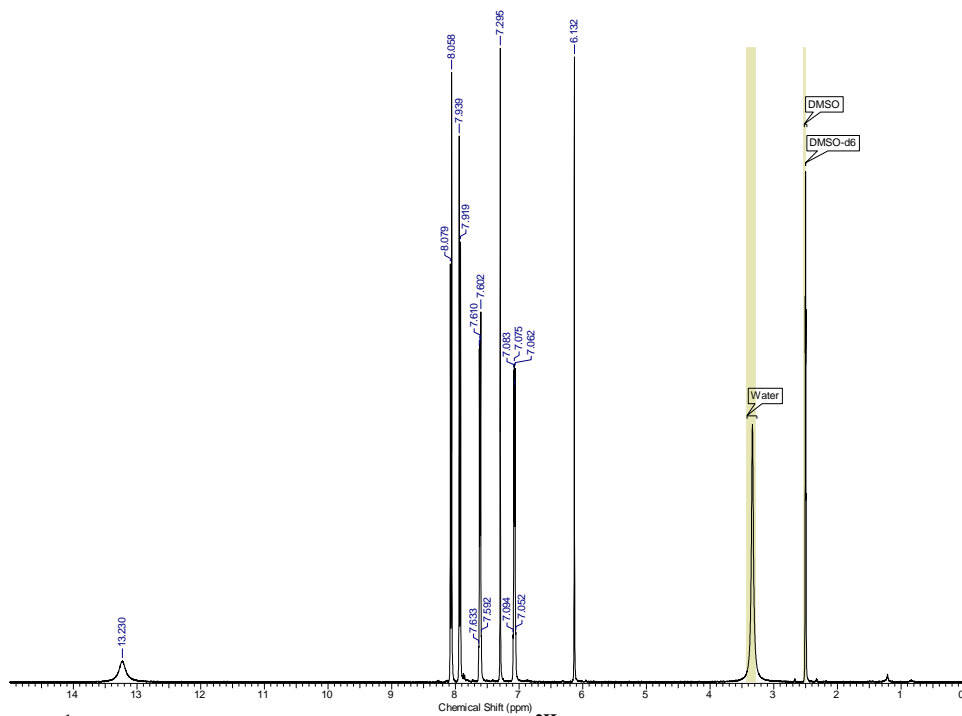


Figure S3. ^1H NMR spectrum of triptycene proligand $1^{2\text{H}}$ (d_6 -DMSO, 298 K, 400 MHz).

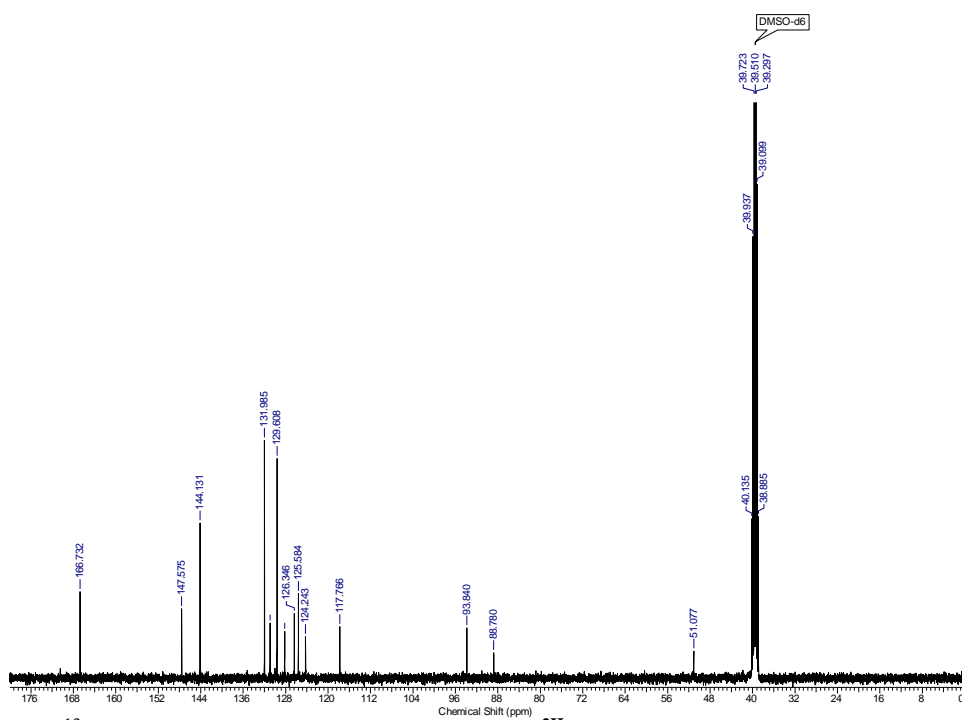


Figure S4. ^{13}C NMR spectrum of triptycene proligand $1^{2\text{H}}$ (d_6 -DMSO, 298 K, 100 MHz).

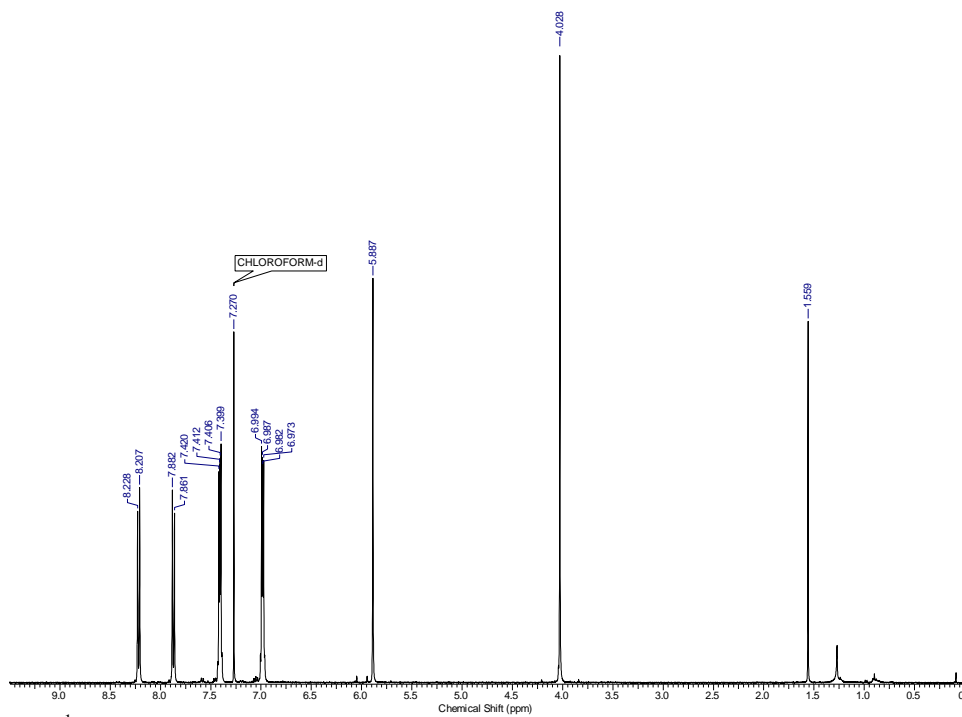


Figure S5. ^1H NMR spectrum of pentiptycene diester **6** (CDCl_3 , 298 K, 400 MHz).

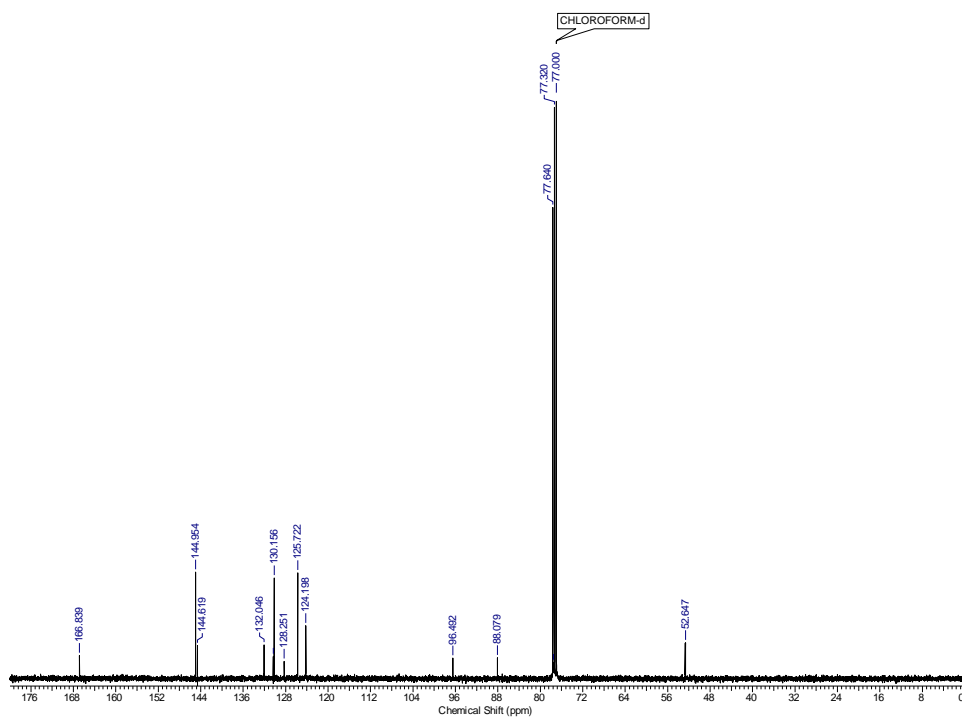


Figure S6. ^{13}C NMR spectrum of pentiptycene diester **6** (CDCl_3 , 298 K, 100 MHz).

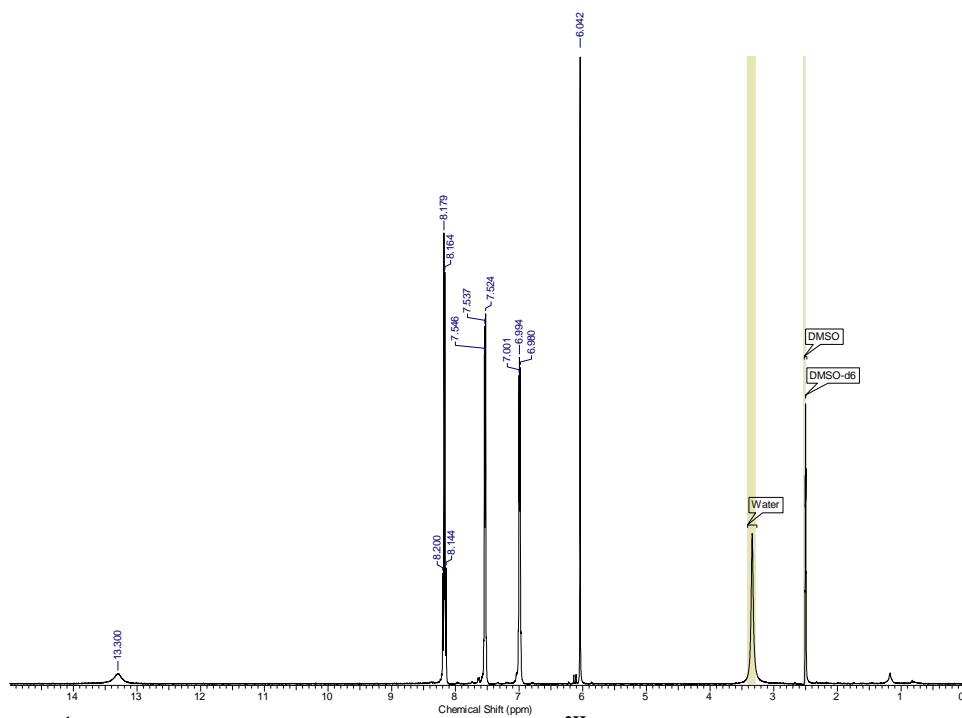


Figure S7. ^1H NMR spectrum of pentiptycene proligand $2^{2\text{H}}$ (d_6 -DMSO, 298 K, 400 MHz).

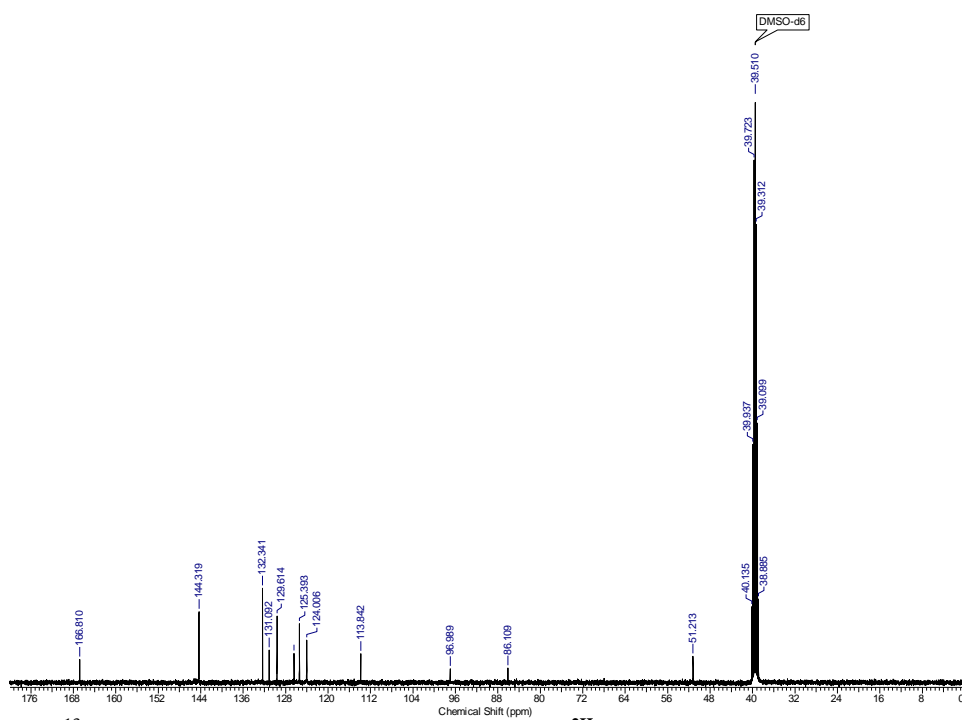


Figure S8. ^{13}C NMR spectrum of pentiptycene proligand $2^{2\text{H}}$ (d_6 -DMSO, 298 K, 100 MHz).

Powder X-ray diffraction spectra of PMOFs

PXRD patterns are presented for **PMOF-2a**, **PMOF-2b** and **PMOF3** below. In each case, the spectrum simulated from the SCXRD data is presented, as well as the spectrum from the bulk sample of crystalline material, and the spectrum after solvent-exchange with dichloromethane followed by air drying.

Generally, the bulk samples show overall crystallinity, and the PXRD spectra show reasonable correlation with the simulated spectra, but crystallinity is lost on attempting to remove solvent from the MOFs.

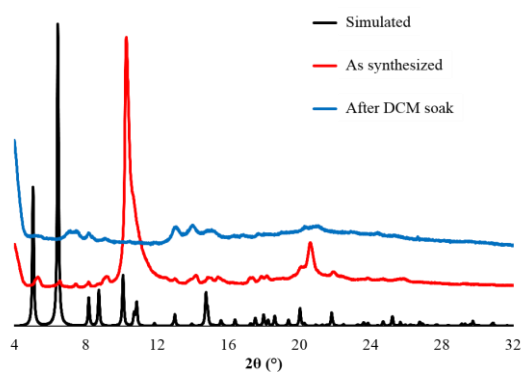


Figure S9. PXRD patterns of **PMOF-2a**: simulated from SCXRD data, as synthesized and after soaking in CH_2Cl_2 .

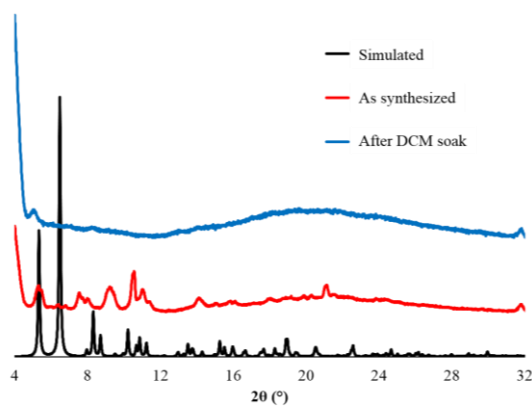


Figure S10. PXRD patterns of **PMOF-2a**: simulated from SCXRD data, as synthesized and after soaking in CH_2Cl_2 .

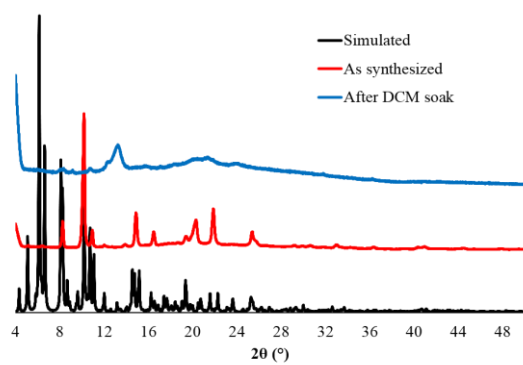


Figure S11. PXRD patterns of **PMOF-3**: simulated from SCXRD data, as synthesized and after soaking in CH_2Cl_2 .

Thermogravimetric analysis of PMOFs

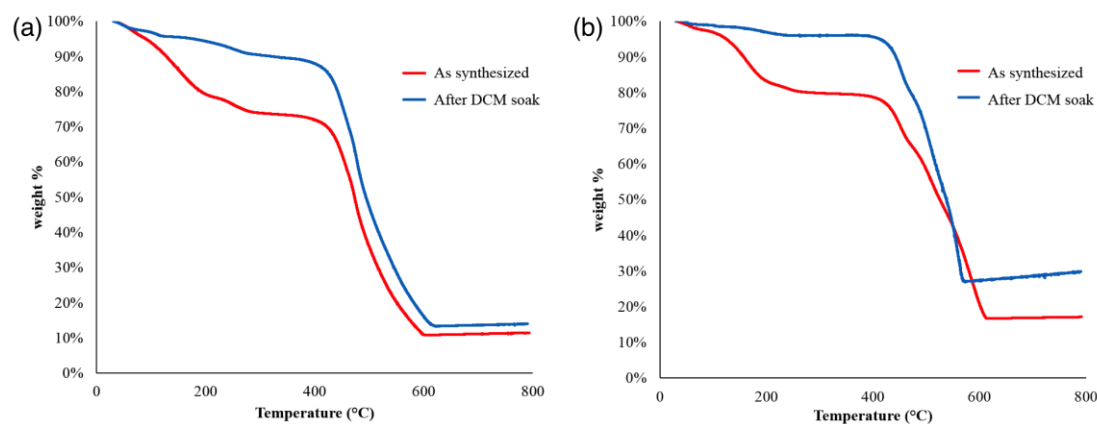


Figure S12. TGA traces as-synthesized and after soaking in CH_2Cl_2 of (a) **PMOF-2a** and (b) **PMOF-2b**.

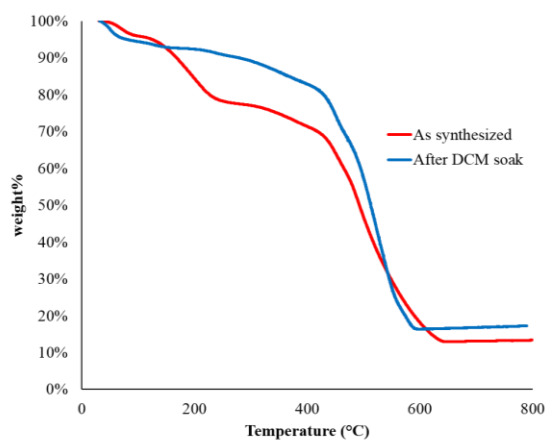


Figure S13. TGA traces as-synthesized and after soaking in CH_2Cl_2 of **PMOF3**.

Reaction of 1^{2H} with $Zn(NO_3)_2 \cdot 6H_2O$

Synthesis

A solution of 1^{2H} (0.0511 g, 0.0942 mmol) and $Zn(NO_3)_2 \cdot 6H_2O$ (0.0839g, 0.282 mmol) in DMF (10 mL) was prepared and transferred to a 23 mL Teflon-lined autoclave by filtering the solution through a puck of celite. The reaction vessel was sealed and heated to 110 °C for 72 h. Slow cooling ($0.1 \text{ } ^\circ\text{C min}^{-1}$ from 110 °C to 25 °C) afforded a clear, yellow solution containing a white crystalline solid, which was isolated by filtration, washed with DMF and dried. Yield: 0.045 g (74%).

IR (cm^{-1}): 2929, 1659, 1601, 1544, 1476, 1458, 1406, 1385, 1252, 1175, 1161, 1093, 1016.862, 808, 780, 707, 639, 587, 517, 474.

Analysis

Bulk sample studies were conducted using PXRD, and thermal stability was probed using TGA (Figure S14). The bulk sample showed poor crystallinity, as was expected by observation of the sample under a microscope. More importantly, however, the peaks that were present did not match with any of the **PMOF-2a** or **PMOF-2b** peaks, leading to the conclusion that this material is not isorecticular and has a different framework structure. Upon desolvation of the sample by soaking in DCM for eight hours, the sample retained the same level of crystallinity, with peaks at $2\theta = 4.5^\circ$, 8.4° and 8.9° becoming sharper and better defined. This suggests that while the framework structure cannot be elucidated, the structure is robust and does not collapse as seen with **PMOF-2a** and **PMOF-2b**. Looking at the TGA traces, as expected a large weight loss is observed below 200 °C. This is most likely due to the loss of encapsulated non-coordinating solvent within the lattice of the material, as observed in **PMOF-2a**, **PMOF-2b**, and **PMOF-3**. Thermal decomposition of the material's organic components does not begin until approximately 420 °C, which is consistent with the pentiptycene MOFs.

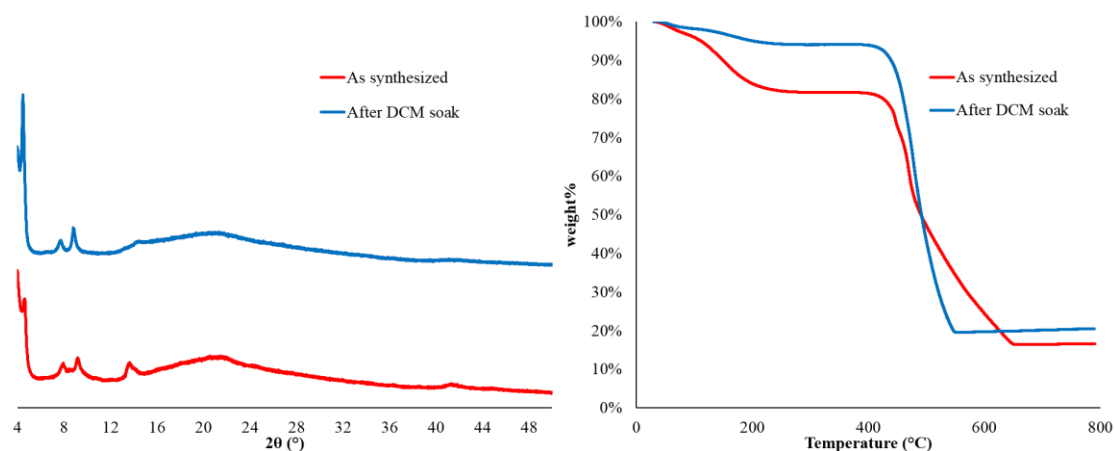


Figure S14. PXRD patterns (left) and TGA traces (right) of product synthesized from the reaction of 1^{2H} $Zn(NO_3)_2 \cdot 6H_2O$ (red: as-synthesized, blue: after soaking in DCM).

For the desolvated material, a small weight loss is apparent lower than 200 °C, once again probably due to the loss of encapsulated non-coordinating solvent. Following that there is no major weight loss until the material undergoes thermal decomposition at 420 °C. The lack of any other weight loss features suggests that unlike in **PMOF-2a**, **PMOF-2b**, and **PMOF-3**, there are no capping ligands (DMF or H₂O) present in the structure of the material, further supporting the proposed formation of a different framework than those previously observed with these ligand analogues.